Direct numerical simulation of Nusselt number scaling in rotating Rayleigh-Bénard convection

G.L. Kooij (g.l.kooij@utwente.nl)[a,*], M.A. Botchev[b], B.J. Geurts[a,c]

[a]*Multiscale Modeling and Simulation, Faculty EEMCS, University of Twente, Enschede, Netherlands*
[b]*Mathematics of Computational Science, Faculty EEMCS, University of Twente, Enschede, Netherlands*
[c]*Faculty of Applied Physics, Fluid Dynamics Laboratory, Eindhoven University of Technology, Eindhoven, Netherlands*

Abstract

We report results from Direct Numerical Simulation (DNS) of rotating Rayleigh-Bénard convection, regarding the scaling of heat transfer with the Rayleigh number for rotating systems at a fixed rate of rotation. The Prandtl number, $Pr = 6.4$, is kept constant. We perform simulations, using a spectral element method, for Rayleigh numbers Ra from 10^6 to 10^9, and Rossby numbers Ro from 0.09 to ∞. We find that the Nusselt number Nu scales approximately with a power 2/7 of Ra at sufficiently high Ra for all Ro. The value of Ra beyond which this Nusselt scaling is well established increases with decreasing Ro. Depending on the rotation rate, the Nusselt number can increase up to 18% with respect to the non-rotating case.

Keywords: Rayleigh-Bénard convection, rotation, heat transfer, direct numerical simulation, turbulence

1. Introduction

Convective heat transfer plays a major role in a wide range of physical phenomena and engineering applications. Rayleigh-Bénard convection is a classic example of convective heat transfer, stimulated by its accessibility to numerical and experimental analysis. In this particular problem, a layer of fluid is heated from below and cooled from above. The thermal expansion of the fluid creates a buoyant force that leads to the convection of heat. We use Direct Numerical Simulation (DNS) to investigate the dependence of the heat transfer efficiency in case the system is in a state of steady rotation.

For the *non-rotating* case the heat transfer, as characterised by the Nusselt number Nu, is predicted to scale with the Rayleigh number Ra as Ra^β in the limit of sufficiently high Ra (Grossmann and Lohse (2000)). In this paper we present results of an extensive parameter study indicating that asymptotically at high Ra, this scaling of the Nusselt number also accurately describes the *rotating* case. Rotation is shown to introduce considerable variation in the flow structuring (Kunnen et al. (2006)). Nevertheless, the simulation results indicate that the scaling exponent β is quite independent of the rotation rate. The main effect of rotation appears through its influence on the value of Ra beyond which the Nusselt number scaling is well expressed.

Rotating Rayleigh-Bénard convection serves as a primary model for understanding the mechanisms of geo- and astrophysical flows. For example, convection inside the core of stars and planets, like the Earth, is believed to generate magnetic fields by a dynamo action (King et al. (2010)). Another example of convection is found in the Earth's atmosphere (Hartmann et al. (2001)), and in the core of the Sun (Miesch (2005)). The efficiency with which heat is transported, measured by the Nusselt number, plays an important role in these natural flow phenomena.

Geo- and astrophysical flows are accompanied by the natural rotation of the respective star or planet. Experiments by, e.g., Liu and Ecke (2009), and Niemela et al. (2010), show that the heat transfer can be affected by rotation. Both physical experiments and numerical simulations are limited in the range of flow scales that can be reproduced. Typically, the interest is in investigating the relevance of scaling laws to extrapolate the Nusselt number to Rayleigh numbers of practical interest. Here, we focus in particular on the effect of rotation on these

---

*Corresponding author

scaling laws, also to provide reference material for a possible extension to rotating systems of the theory put forward in Grossmann and Lohse (2000) for the non-rotating case.

There are various studies of the Nusselt number as function of the rotation rate, i.e., the inverse Rossby number (Horn and Shishkina, 2014; Kunnen et al., 2008, 2011; Stevens et al., 2009; Zhong et al., 2009). We can roughly distinguish three regimes with respect to the Rossby number. In the weak-rotation regime ($Ro \gtrsim 2.5$), the flow is dominated by a large-scale circulation. The Nusselt number does not increase with respect to the non-rotating case. In the moderate-rotation regime ($0.15 \lesssim Ro \lesssim 2.5$), the large-scale circulation breaks down due to rotation, and the flow organizes itself in vertically aligned vortices. The Nusselt number increases with the rotation rate. Finally in the strong-rotation regime ($Ro \lesssim 0.15$), rotation dominates the flow structure and suppresses heat transport in the vertical direction. The Nusselt number rapidly decreases with the rotation rate.

In this numerical study, we consider Rayleigh-Bénard convection in a rotating vertical cylinder with a width-to-height aspect ratio $\Gamma = D/L = 1$. The goal is to study the influence of the temperature difference between top and bottom walls (characterised by the Rayleigh number) and the rotation rate (characterised by the Rossby number) on the structure of the flow and the heat transfer. We perform direct numerical simulations for a wide range of Rossby and Rayleigh numbers to investigate the dependence of the Nusselt number. The direct numerical simulations are performed with a spectral element method, implemented in the open-source code *Nek5000*, originally developed by Fischer (1997). The purpose of this work is essentially twofold. On the one hand, we assess the performance of the spectral-element method in direct numerical simulations of Rayleigh-Bénard convection. On the other hand, we seek a deeper understanding of the effect of rotation on the transition from an unsteady laminar flow to a developed turbulent flow when increasing the Rayleigh number.

The organization of this paper is as follows. We first discuss, in Section 2, the governing equations for Rayleigh-Bénard convection including rotation. In Section 3, we briefly describe the spectral element method used for DNS and justify the spatial resolution we used. Numerical findings are presented in Section 4 in which we establish the dependence of the heat transfer on the Rayleigh and

Rossby number. We show that the Nusselt number asymptotically maintains strong scaling with the Rayleigh number also in case of rotation, and that rotation and the temperature difference qualitatively change the flow. Concluding remarks are collected in Section 5.

2. Boussinesq approximation of rotating Rayleigh-Bénard convection

This section describes the equations of motion, regarding Rayleigh-Bénard convection in a rotating cylinder and the evaluation of the Nusselt number from the simulation data.

2.1. Rotating coordinate system

The effect of rotation is taken into account by adopting a co-rotating coordinate system and recasting Newton's laws into this non-inertial coordinate system. The adoption of such a coordinate system introduces additional (fictitious) body forces. We derive the effects of rotation on the evolution of the flow and start from the Navier-Stokes equation in the inertial coordinate system,

$$\rho(\partial_t + \mathbf{v} \cdot \nabla)\mathbf{v} = -\nabla p + \mu \nabla^2 \mathbf{v} + \rho \mathbf{g}. \qquad (1)$$

Here, ρ is the density, $\mathbf{v}$ the velocity, p the pressure, μ the molecular viscosity and $\mathbf{g}$ the gravitational acceleration. Following the approach by Kundu and Cohen (2010), we make use of the kinematic relation,

$$\mathbf{v} = \mathbf{u} + \mathbf{\Omega} \times \mathbf{r}. \qquad (2)$$

Here, $\mathbf{u}$ and $\mathbf{r}$ are the velocity and position vector in the co-rotating coordinate system, and $\mathbf{\Omega}$ is the rotation vector. Substituting relation (2) into the Navier-Stokes equation (1) yields after a little manipulation,

$$\begin{aligned}
\rho(\partial_t + \mathbf{u} \cdot \nabla)\mathbf{u} = &-\nabla p + \mu \nabla^2 \mathbf{u} + \rho \mathbf{g} \\
&- 2\rho\, \mathbf{\Omega} \times \mathbf{u} \\
&- \rho\, \mathbf{\Omega} \times (\mathbf{\Omega} \times \mathbf{r}).
\end{aligned} \qquad (3)$$

The rotation of the non-inertial coordinate system introduces two fictitious (or *d'Alembert*) forces, which are the Coriolis force ($2\rho\, \mathbf{\Omega} \times \mathbf{u}$) and the centrifugal force ($\rho\, \mathbf{\Omega} \times (\mathbf{\Omega} \times \mathbf{r})$).

In our study, we consider Rayleigh-Bénard in a cylinder rotating about its vertical axis, as illustrated in Fig. 1. The coordinate system rotates along with the cylinder and the rotation vector is $\mathbf{\Omega} = (0, 0, \Omega)^T$, where Ω is simply the rate of rotation.
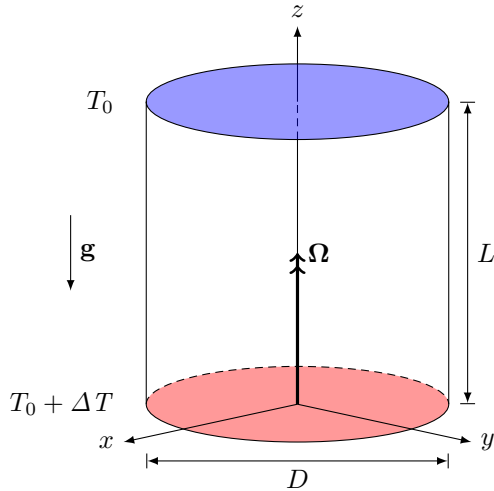
Figure 1: Geometry of the rotating cylinder.

2.2. Boussinesq approximation

Rayleigh-Bénard convection is driven by a temperature difference between the "warm" and "cold" plate. The thermal expansion of the fluid generates buoyancy that sets the fluid in motion. This effect of compressibility can be simplified by the *Boussinesq approximation*. In essence, the fluid is regarded to be incompressible and only the leading-order effects of compressibility are taken into account. A comprehensive description of the Boussinesq approximation is given by Landau and Lifshitz (1987). To start with, we consider a density variation ρ' from a reference density ρ_0, $\rho = \rho_0 + \rho'$. The variation in density is assumed to be small in the sense that $\rho'/\rho_0 \ll 1$. Typically, we need an equation of state to close the governing equations. Here, the equation of state is approximated by,

$$\rho = \rho_0 \left[1 - \beta(T - T_0)\right], \qquad (4)$$

where β is the thermal expansion coefficient and T_0 a reference temperature, taken equal to the temperature of the upper plate. This linearisation is only accurate for small fluctuations in temperature, relative to the reference temperature. By substituting (4) into the Navier-Stokes equation (3) and collecting terms of similar magnitude, we find,

$$\rho_0(\partial_t + \mathbf{u} \cdot \nabla)\mathbf{u} = -\nabla q + \mu\nabla^2\mathbf{u} - \rho_0\beta(T - T_0)\mathbf{g}$$
$$- 2\rho_0 \, \boldsymbol{\Omega} \times \mathbf{u}$$
$$+ \rho_0\beta(T - T_0)\boldsymbol{\Omega} \times (\boldsymbol{\Omega} \times \mathbf{r}). \quad (5)$$

Here, we define an effective pressure $q = p + \rho_0\phi - \rho_0|\Omega \times \mathbf{r}|^2/2$, where ϕ is a scalar field related to

gravity $\mathbf{g} = -\nabla\phi$. The concise notation q is possible since the hydrostatic components of the gravitational and centrifugal force can written as a gradient. Additionally, we have the energy and continuity equation,

$$\rho C_p(\partial_t + \mathbf{u} \cdot \nabla)T = k\nabla^2 T, \qquad (6)$$
$$\nabla \cdot \mathbf{u} = 0. \qquad (7)$$

Here, C_p is the specific heat coefficient at constant pressure, and k the thermal conductivity. The governing equations are complemented by the boundary conditions listed in Table 1. A no-slip condition is imposed at the wall and the side-wall of the cylinder is assumed to be perfectly insulated, while at the top and bottom walls the temperature is prescribed.

The Boussinesq approximation was first discovered by Oberbeck (1879), but is generally attributed to Boussinesq (1903). The Boussinesq approximation is a common practice motivated by cases with relatively small temperature differences of a few degrees Kelvin between the top and bottom walls. The exact validity of this approximation is examined in close detail by, e.g., Gray and Giorgini (1976). One of the necessary assumptions is that fluid properties, μ, k, and β, are independent of temperature. The additional effects of temperature-dependent viscosity and thermal diffusivity are for example studied by Ahlers et al. (2006).

Table 1: Boundary conditions

Bottom plate	$\mathbf{u} = 0$	$T = T_0 + \Delta T$
Top plate	$\mathbf{u} = 0$	$T = T_0$
Side-wall	$\mathbf{u} = 0$	$\frac{\partial T}{\partial \mathbf{n}} = 0$

2.3. Dimensionless formulation

Following earlier work by Kunnen et al. (2010) for example, we use the height of the cylinder L as the reference length and the *free-fall velocity* $U = \sqrt{g\beta\Delta T L}$ as the reference velocity. Using these typical scales, the governing equations take

3

the dimensionless form,

$$(\partial_t + \mathbf{u} \cdot \nabla) \mathbf{u} = - \nabla q + (Pr/Ra)^{1/2} \nabla^2 \mathbf{u} + T \mathbf{e}_z$$
$$- (1/Ro) \mathbf{e}_z \times \mathbf{u}$$
$$+ Fr T \, \mathbf{e}_z \times (\mathbf{e}_z \times \mathbf{r}), \tag{8a}$$
$$(\partial_t + \mathbf{u} \cdot \nabla) T = (PrRa)^{-1/2} \nabla^2 T, \tag{8b}$$
$$\nabla \cdot \mathbf{u} = 0. \tag{8c}$$

Here, we have used $\mathbf{g} = -\mathbf{e}_z$, $\mathbf{\Omega} = \mathbf{e}_z$, and the unit vector $\mathbf{e}_z = (0,0,1)^T$. The equations are solved numerically in the dimensionless formulation, together with the dimensionless boundary conditions listed in Table 2. In the remaining sections, we implicitly assume that quantities are dimensionless unless stated otherwise.

We can identify four dimensionless numbers that characterize rotating Rayleigh-Bénard convection,

$$Ra = g\beta\Delta T L^3/(\nu\kappa), \tag{9}$$
$$Pr = \nu/\kappa, \tag{10}$$
$$Ro = U/(2\Omega L), \tag{11}$$
$$Fr = \Omega^2 L/g, \tag{12}$$

which are the Rayleigh, Prandtl, Rossby and Froude number respectively. In the present study, we assume that $Fr \ll 1$ and the temperature-dependent component of the centrifugal force can be neglected. A study by Zhong et al. (2009) shows this assumption is valid for a range of realistic configurations. In the experimental study by Kunnen et al. (2010), we find $Fr < 0.04$ for example.

Table 2: Dimensionless boundary conditions

Bottom plate	$\mathbf{u} = 0$	$T = 1$
Top plate	$\mathbf{u} = 0$	$T = 0$
Side-wall	$\mathbf{u} = 0$	$\frac{\partial T}{\partial \mathbf{n}} = 0$

The dynamics of rotating Rayleigh-Bénard convection is characterized by the combination of the said dimensionless parameters. A critical Rayleigh number Ra_c indicates the onset of convection (Hébert et al., 2010), beyond which the hydrostatic equilibrium is no longer stable. Higher Rayleigh numbers lead eventually to a regime from "soft" to "hard" turbulence (Julien et al., 1996a).

In combination with the buoyancy effects driving Rayleigh-Bénard convection, rotation can have a signficant influence on the overall flow structuring (Kunnen et al., 2006). Early experimental research by Rossby (1969) shows that rotation could increase the heat transfer with respect to the non-rotating case. This increase in heat transfer is associated with a qualitative change in the structure of the flow. A relevant parameter is Rossby number: the ratio of the inertial to the Coriolis force. At high Rossby numbers, i.e., very slow rotation, the effect of rotation is limited and the flow is dominated by a *large-scale circulation* (LSC) (Kunnen et al., 2008). For sufficiently low Rossby numbers, the Coriolis force becomes dominant and is capable of breaking up the LSC. In that case, local vortical structures occur, penetrating well into the domain from both the top and the bottom walls. These structures are characteristic of conditions that display a strongly increased transport of heat due to Ekman pumping (Ekman, 1905).

In this paper we consider a system composed of water and take $Pr = 6.4$ throughout. The Rayleigh number is varied ranging from 10^6 to 10^9, while the Rossby number is varied from ∞ for the non-rotating case to values as low as ≈ 0.1.

2.4. Global heat transfer

The purpose of the direct numerical simulations is to measure the global heat transfer by the flow. The Nusselt number, which is the ratio between the total and the conductive heat flux, provides the following expression of the local heat transfer (here taken in the vertical direction),

$$Nu = (PrRa)^{1/2} u_z T - \partial_z T. \tag{13}$$

The global heat transfer is measured, either by averaging over the walls of the cylinder or the entire volume. The wall- and volume-averaged Nusselt numbers are as follows,

$$\langle Nu \rangle_W = \langle \partial_z T \rangle_W \tag{14}$$
$$\langle Nu \rangle_V = 1 + (PrRa)^{1/2} \langle u_z T \rangle_V \tag{15}$$

where $\langle . \rangle_W$ and $\langle . \rangle_V$ denotes the average over the walls and the volume, respectively. Here, we have already simplified the averages with the boundary conditions given in Table 2, following a similar approach by Kerr (1996). Both averages should agree if the averaging time and the spatial resolution are sufficient. Naturally, the Nusselt number of the bulk is sensitive to the resolution in the bulk, and the Nusselt number of the wall to the resolution in the near-wall regions. This provides an extra, a posteriori, check on the spatial resolution used in the numerical simulations.

3. Spectral element method

The governing equations, given by Eq. (8), are solved numerically with the spectral element method (SEM), that is implemented in the open-source code *Nek5000* (Fischer, 1997). The spectral element method is essentially a variation of the finite element method using higher-order piecewise polynomials as basis functions. Deville et al. (2004) describe in more detail the spectral element method and its application to fluid dynamics.

The basis functions of the velocity are local tensor-product Lagrange interpolants of order p on Gauss-Lobatto-Legendre nodes, whereas the basis functions of the pressure are Lagrange interpolants of order $p - 2$ on Gauss-Legendre nodes. The total number of grid points is then $(p + 1)^3$ (for the velocity) per three-dimensional element.

For time-integration, a semi-implicit third-order BDF3/EXT3 scheme is used (Karniadakis et al., 1991). The viscous term is intregrated with a third-order backward differencing scheme (BDF3), and the nonlinear convective term with a third-order extrapolation scheme (EXT3). In general, we use adaptive time-stepping with a target CFL number of 0.5, which is in practice more than sufficient to guarantee the stability during the simulation. A CFL number of $\lesssim 1$ is usually advocated (Deville et al., 2004).

In turbulent flows at high Rayleigh numbers the physics is dominated by convection, as opposed to diffusion in laminar flows. Rønquist (1996) shows that skew-symmetry of the convective operator is crucial for the stability of the numerical scheme. Malm et al. (2013) demonstrate that the skew-symmetry of the convective operator can be respected by *over-integration*, which means applying quadrature rules with orders higher than N. Quadrature rules of order $3N/2$, instead of N, are in practice sufficient to approximate the skew-symmetry of the convective operator up to machine precision. Over-integration is indispensable to stabilizing the SEM in convection-dominated flows and, consequently, is applied in the numerical simulations presented in this study.

In this numerical study, we use spectral elements with polynomial order $p = 5$. We perform a convergence test to determine the required number of elements, i.e., spatial resolution, for accurate estimates of the Nusselt number. Here, the mesh is characterized by the number of elements in the z-direction, E_z, and in the xy-plane, E_{xy}. We

Table 3: Number of spectral elements in z-direction, E_z, and in the xy-plane, E_{xy}, with their respective average mesh widths $\bar{h}_z$ and $\bar{h}_{xy}$.

Mesh	E_z	$\bar{h}_z$	E_{xy}	$\bar{h}_{xy}$
1	16	$6.250 \cdot 10^{-2}$	300	$4.976 \cdot 10^{-2}$
2	24	$4.167 \cdot 10^{-2}$	588	$3.555 \cdot 10^{-2}$
3	32	$3.125 \cdot 10^{-2}$	972	$2.766 \cdot 10^{-2}$
4	48	$2.083 \cdot 10^{-2}$	1728	$2.078 \cdot 10^{-2}$

performed several simulations for $Ra = 10^8$ and $Ra = 10^9$ with the different resolutions given in Table 3. To capture the sharp gradients in the boundary layers, the meshes are refined in the near-wall region. The grids used in this study vary from about 10^6 degrees of freedom ($E_z \times E_{xy} \times (p + 1)^3$) to $\approx 1.8 \, 10^7$.

The goal here is to find an appropriate resolution for the simulations presented in the remaining sections. We assume that cases with the highest rotation rate of $Ro = 0.09$ are the most demanding cases in terms of spatial resolution. We run several simulations for the two Rayleigh numbers, $Ra = 10^8$ and $Ra = 10^9$. The simulations run for a total of 300 time units, starting from a zero-velocity field and a linear temperature profile ($T = z$) as initial conditions. The Nusselt number is only averaged over the last 200 time units, in which the flow has reached an approximately statistically stationary state. We estimate a 95% confidence bound by taking uncorrelated samples from the available history and calculating the standard mean error. The Nusselt numbers for different resolutions are given in Table 4.

For $Ra = 10^8$, both Nusselt numbers, $\langle Nu \rangle_V$ and $\langle Nu \rangle_W$, are seen to have converged with the second and third mesh, and agree within their uncertainty bounds. The results also suggest that a higher resolution is required in the case that $Ra = 10^9$. From these results, the formal order of convergence cannot be established given the statistical errors in the time-averaged Nusselt number. The value of $\langle Nu \rangle_V$ appears to be more sensitive than $\langle Nu \rangle_W$ to the number of elements used. The slow convergence of $\langle Nu \rangle_V$ in comparison with $\langle Nu \rangle_W$ could be explained by the relatively lower resolution in the bulk, due to the significant mesh refinement near the wall. Based on these results, we decide to use the third resolution for $Ra \leq 10^8$, and the fourth for $Ra = 10^9$.

Table 4: Convergence of the time-averaged Nusselt number with increasing spatial resolution, in the case $Ro = 0.09$.

Ra	Mesh	$\langle Nu \rangle_W$	$\langle Nu \rangle_V$
10^8	1	37.5 ± 0.4	40.2 ± 1.2
–	2	38.0 ± 0.5	38.1 ± 1.2
–	3	37.9 ± 0.6	38.2 ± 1.6
10^9	1	77.8 ± 0.7	108.5 ± 1.9
–	2	72.2 ± 0.8	88.7 ± 2.2
–	3	73.4 ± 1.0	80.9 ± 3.1
–	4	72.2 ± 0.9	73.8 ± 1.9

Table 5: Time-averaged Nusselt numbers, including the 95% confidence bounds, for $Pr = 6.4$, $\Gamma = 1$ and varying Ra and Ro.

Ra	Ro	$\langle Nu \rangle_W$	$\langle Nu \rangle_V$
10^6	0.09	5.7 ± 0.2	5.5 ± 0.2
10^6	∞	9.0 ± 0.1	9.0 ± 0.1
10^7	0.09	16.0 ± 0.3	16.1 ± 0.5
10^7	0.36	18.8 ± 0.1	18.8 ± 0.4
10^7	1.08	17.3 ± 0.1	17.4 ± 0.3
10^7	∞	16.4 ± 0.1	16.5 ± 0.2
10^8	0.09	37.9 ± 0.3	38.2 ± 0.8
10^8	∞	33.0 ± 0.1	33.2 ± 0.4
10^9	0.09	72.2 ± 0.5	73.8 ± 1.0
10^9	0.36	71.2 ± 0.2	72.2 ± 0.9
10^9	1.08	66.8 ± 0.2	67.0 ± 1.6
10^9	∞	64.5 ± 0.3	66.5 ± 1.8

4. Heat transfer scaling and flow structure

In this section, we first analyze the scaling of the Nusselt number with the Rayleigh number, under influence of steady rotation in Subsection 4.1. We show that the Nusselt number increases up to 15% with respect to the non-rotating case, depending on the rate of rotation. Subsequently, in 4.2 we illustrate the qualitative changes in the flow structure as a result of changes in Ra and Ro.

4.1. Scaling of the heat transfer under rotation

In general, we are interested in scaling laws of the form, $Ra = \alpha Nu^\beta$. A universal law that covers the entire parameter space, does not exist, as the coefficients α and β depend on the dimensionless parameters themselves. Grossmann and Lohse (2000) propose a comprehensive theory of scaling laws that accounts for different regimes in the (Ra, Pr) parameter space. The boundaries between these regimes are not sharp, allowing for transitional scaling laws to prevail. Experiments for low Prandtl numbers by Castaing et al. (1989) show that the exponent $\beta = 2/7$ holds in a large range of Rayleigh numbers ($Ra > 4 \cdot 10^7$). The existence of a 2/7-regime is theoretically supported by Shraiman and Siggia (1990). Regarding rotating Rayleigh-Bénard convection, the question arises: is there a scaling law, $Nu \propto Ra^\beta$? If so, what is the scaling exponent β?

We run simulations for 300 time units, starting with a zero-velocity field and a linear temperature profile ($T = z$) as initial conditions. The Nusselt number of the wall, $\langle Nu \rangle_W$, and of the volume, $\langle Nu \rangle_V$, are averaged over the last 200 time units, in which the flow has reached a statistically stationary state. The time-averaged values of Nu are given in Table 5, in which Ra varies from 10^6 to 10^7 and Ro from 0.09 to ∞. For each simulation,

the two Nusselt numbers agree within the 95% confidence bounds. The convergence study presented in Section 3, suggests that this is an indication of numerical convergence with respect to the spatial resolution of the simulations. Using these grids, the main structures in the flow associated with heat transfer, e.g., boundary layers near all vertical and horizontal walls, appear well captured.

The convergence study in Section 3 also shows that $\langle Nu \rangle_W$ converges faster than $\langle Nu \rangle_V$, when increasing the resolution. The time-average of $\langle Nu \rangle_W$ has a smaller statistical error too. In the remainder of this paper, we evaluate Nu via $\langle Nu \rangle_W$, as it appears more robust, both numerically *and* statistically, than $\langle Nu \rangle_V$.

The scaling of the Nusselt number with the Rayleigh number is illustrated by plotting the data in a logarithmic scale in Fig. 2. We compare the results to the theoretical scaling for non-rotating Rayleigh-Bénard convection by Grossmann and Lohse (2000), with the updated prefactors by Stevens et al. (2013). The results for the non-rotating case, $Ro = \infty$, agree closely with the theoretical predictions. In addition, we observe that the Grossmann-Lohse theory can be approximated with a 2/7 power law in a certain range of Rayleigh numbers. A least squares fit in the range $10^7 \le Ra \le 10^9$, and $Ro = \infty$, produces the power law $Nu \approx 0.15 Ra^{0.29}$, which is close to the theoretical exponent of 2/7. This result is also in close agreement with the scaling $Nu = 0.145 Ra^{0.294}$, observed in direct numerical simulations by Bailon-

Cuba et al. (2010). Those results were obtained with a finite volume method, used by several groups working in the field of Rayleigh-Bénard convection (Verzicco and Orlandi, 1996; Verzicco and Camussi, 2003). In the lower range $Ra \lesssim 10^7$ the scaling exponent deviates slightly from 2/7. This range of Rayleigh numbers is characterized by "soft" turbulence, in which a 2/7 power law does not hold (Castaing et al., 1989).

The scaling of Nu with Ra is shown in more detail in Fig. 3. Here, we have compensated the Nusselt number by a presumed scaling exponent of 2/7. The effect of *rotation* on the scaling of Nu is not entirely straightforward. As for the non-rotating case, a single power law seems to be inadequate in describing the scaling of Nu in the entire range of Rayleigh numbers. For $Ra \gtrsim 10^8$, the scaling appears to be similar to 2/7, for all Rossby numbers. The existence of a 2/7 power law in rotating Rayleigh-Bénard convection was also observed in other experiments and simulations (Julien et al., 1996b; Liu and Ecke, 1997), independent of the Rossby number. Our results do suggest a weak dependence on the Rossby number. The scaling exponent in the range $10^8 \lesssim Ra \lesssim 10^9$ subtly decreases with the inverse Rossby number. At $Ro = 0.36$ and $Ro = 0.09$ we observe scaling exponents that are slightly below 2/7. Because of limited computational resources, we have not been able to explore the range $Ra > 10^9$ yet. For $Ra \lesssim 10^7$ we do not observe a uniform scaling at all. At these low Rayleigh numbers various effects of the relatively high viscosity have to be taken into account.

In Fig. 4, the Nusselt number is plotted against the inverse Rossby number. Here, the Nusselt number is normalized by the value of the non-rotating case ($Ro = \infty$) to illustrate the relative increase. The results for $Ra = 10^9$ agree with the DNS data by Kunnen et al. (2008), which are performed for identical physical parameters ($Ra = 10^9$, $Pr = 6.4$, and $\Gamma = 1$). We can also distinguish the three regimes of rotation, described by Kunnen et al. (2011). In the weak-rotation regime, the heat transport does not increase. In the moderate-rotation regime, the Nusselt number increases with the inverse Rossby number. In the strong-rotation regime, the Nusselt number rapidly decreases. This Rossby-number dependence is also observed in experiments by Kunnen et al. (2011) and Zhong et al. (2009).

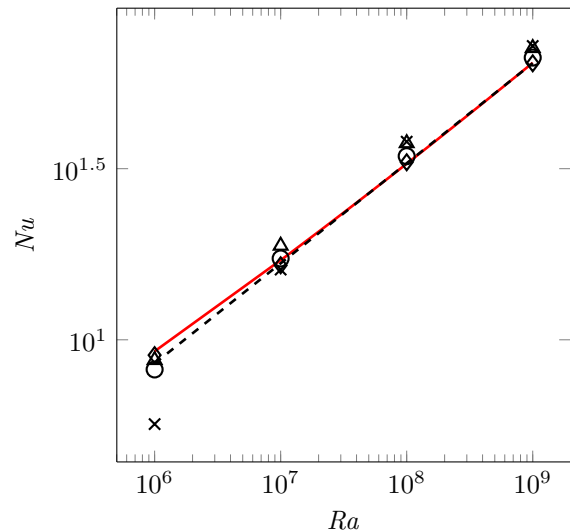We find a maximum increase of 18% at $Ra = 10^7$ and $Ro = 0.18$, and 15% at $Ra = 10^9$ and

Figure 2: Scaling of Nu with Ra. $\diamond$: $Ro = \infty$, $\circ$: $Ro = 1.08$, $\triangle$: $Ro = 0.36$, $\times$: $Ro = 0.09$, dashed: $0.15Ra^{0.29}$ (least squares fit $10^7 \leq Ra \leq 10^9$), solid: GL theory with updated prefactors (Stevens et al., 2013).
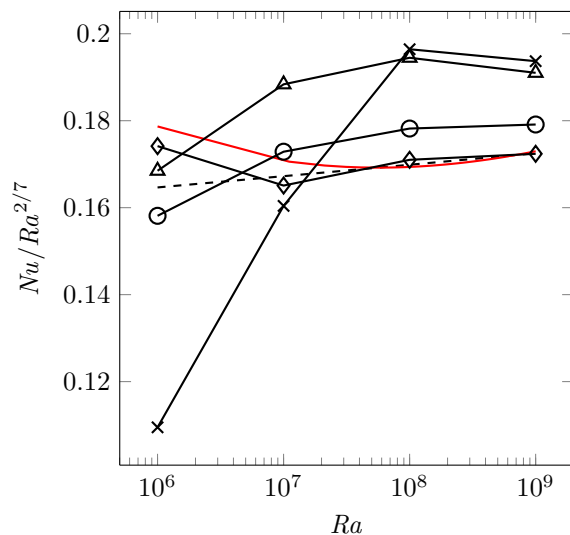

Figure 3: Scaling of Nu with Ra, compensated by $Ra^{2/7}$. $\diamond$: $Ro = \infty$, $\circ$: $Ro = 1.08$, $\triangle$: $Ro = 0.36$, $\times$: $Ro = 0.09$, dashed: $0.15Ra^{0.29}$ (least squares fit $10^7 \leq Ra \leq 10^9$), solid: GL theory with updated prefactors (Stevens et al., 2013).

$Ro = 0.18$. The increase of heat transfer can be attributed to a phenomenon called *Ekman transport*, first described by Ekman (1905). The rotation creates vortices in the boundary layer, that essentially "pump" fluid into the bulk. These vortices provide a more efficient mechanism of transferring heat compared to the pure non-rotating turbulent flow. This is expressed by an increase in the Nusselt number.

The results for $Ra = 10^7$ and $Ra = 10^9$ show a comparable trend in the Nusselt number. For $Ra = 10^7$ the Nusselt number shows initially a stronger increase, but eventually a faster decrease in the strong-rotation regime. The difference might be explained by the fact that, with decreasing Ra, the buoyancy becomes weaker with respect to the Coriolis force. Our results imply that the effect of rotation is more pronounced at lower Rayleigh numbers. A similar observation is made by Weiss and Ahlers (2011).
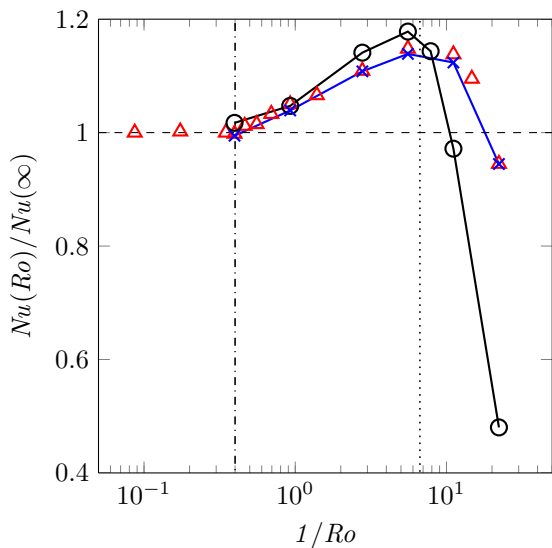

Figure 4: The Nusselt number as function of the inverse Rossby number. The Nusselt number is normalized by its non-rotating value. ∘: $Ra = 10^7$, ×: $Ra = 10^9$, △: DNS for $Ra = 10^9$, $Pr = 6.4$ (Kunnen et al., 2008). The vertical dashdotted line indicates the transition between the weak- and moderate-rotation regime (Weiss and Ahlers, 2011), and the vertical dotted line the transition between the moderate- and strong-rotation regime (Kunnen et al., 2011).

4.2. Change in flow structure

To visualize the effect of the Rayleigh and Rossby numbers on the three-dimensional flow, we compare the velocity and temperature solutions in the non-rotating case ($Ro = \infty$) with the rapidly rotating one ($Ro = 0.09$). Figures 5 and 6 show several snapshots of the temperature and the vertical velocity field for $Ro = \infty$ and $Ro = 0.09$, with Ra ranging from 10^6 to 10^9.

At $Ro = \infty$, convection is dominated by a *large-scale circulation* (Kunnen et al., 2008). Thermal plumes are visible in the temperature field when increasing the Rayleigh number. The flow shows very different patterns at $Ro = 0.09$, i.e., in case of strong steady rotation. Both the temperature and velocity field exhibit long structures in the vertical direction. These structures are generally described as Taylor columns. According to the Taylor-Proudman theorem, the flow tries to align itself with the rotation axis (King and Aurnou, 2012). The vortices are created by Ekman transport in the horizontal boundary layers, which lead to the enhanced tranport of heat away from the wall (Stevens et al., 2009). These vortices become particularly apparent at higher Rayleigh numbers. At $Ra = 10^6$ for example, the effect of rotation is practically indiscernable in the temperature field. These findings corroborate the previous assertion that rotation can increase the heat transfer at $Ra \geq 10^7$, with respect to the non-rotating case.

5. Conclusions

We applied direct numerical simulations, on the basis of a spectral element spatial discretisation method, to study the scaling of heat transport in rotating Rayleigh-Bénard convection in a cylindrical container with aspect ratio $\Gamma = 1$. For $Ro = \infty$, we find $Nu \propto Ra^{0.29}$ in the studied range of $10^6 \leq Ra \leq 10^9$, which matches well with the expected $2/7$ scaling from literature. For $0.09 \leq Ro \leq 1.08$, a similar scaling of the Nusselt number seems to apply in the high Rayleigh number regime of $Ra \gtrsim 10^8$. In this regime, the Nusselt number also increases up to 18% for $Ra = 10^7$ and 15% for $Ra = 10^9$ with respect to non-rotating case. The enhanced heat transport is linked to the vertical vortices, created by the rotation of the system, that are observed in the temperature and the velocity field.

Acknowledgements

(a) $Ra = 10^6$, $Ro = \infty$ (b) $Ra = 10^6$, $Ro = 0.09$

(c) $Ra = 10^7$, $Ro = \infty$ (d) $Ra = 10^7$, $Ro = 0.09$

(e) $Ra = 10^8$, $Ro = \infty$ (f) $Ra = 10^8$, $Ro = 0.09$

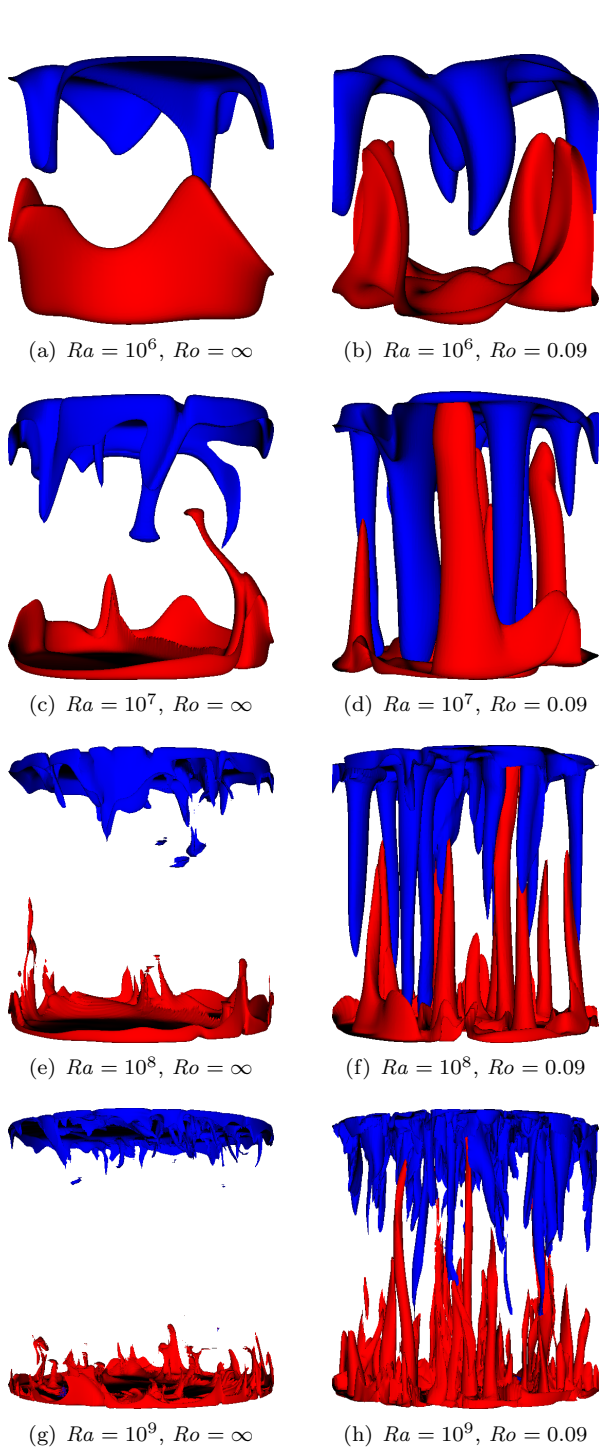(g) $Ra = 10^9$, $Ro = \infty$ (h) $Ra = 10^9$, $Ro = 0.09$

Figure 5: Isosurfaces of temperature field T for Ra from 10^6 to 10^9, and $Ro = \infty$ and $Ro = 0.09$. Red colour corresponds to $T = 0.65$ and blue to $T = 0.35$.

(a) $Ra = 10^6$, $Ro = \infty$ (b) $Ra = 10^6$, $Ro = 0.09$

(c) $Ra = 10^7$, $Ro = \infty$ (d) $Ra = 10^7$, $Ro = 0.09$

(e) $Ra = 10^8$, $Ro = \infty$ (f) $Ra = 10^8$, $Ro = 0.09$

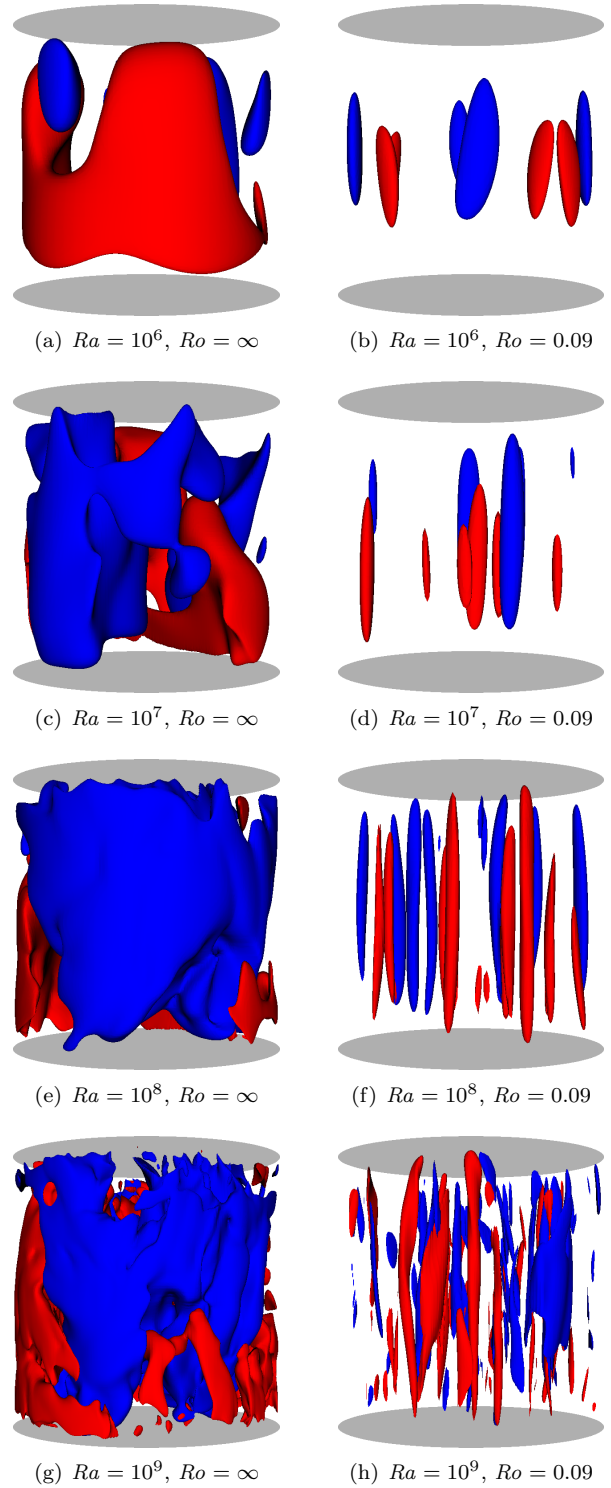(g) $Ra = 10^9$, $Ro = \infty$ (h) $Ra = 10^9$, $Ro = 0.09$

Figure 6: Isosurfaces of vertical velocity field u_z for Ra from 10^6 to 10^9, and $Ro = \infty$ and $Ro = 0.09$. Red colour corresponds to $u_z = 0.07$ and blue to $u_z = -0.07$.

Ahlers, G., Brown, E., Araujo, F. F., Funfschilling, D., Grossmann, S., Lohse, D., 2006. Non-Oberbeck–Boussinesq effects in strongly turbulent Rayleigh–Bénard convection. Journal of Fluid Mechanics 569, 409–445.

Bailon-Cuba, J., Emran, M. S., Schumacher, J., 2010. Aspect ratio dependence of heat transfer and large-scale flow in turbulent convection. Journal of Fluid Mechanics 655, 152–173.

Boussinesq, J., 1903. Théorie analytique de la chaleur: mise en harmonie avec la thermodynamique et avec la théorie mécanique de la lumière. Vol. 2. Gauthier-Villars.

Castaing, B., Gunaratne, G., Heslot, F., Kadanoff, L., Libchaber, A., Thomae, S., Wu, X.-Z., Zaleski, S., Zanetti, G., 1989. Scaling of hard thermal turbulence in Rayleigh-Bénard convection. Journal of Fluid Mechanics 204, 1–30.

Deville, M., Fischer, P., Mund, E., 2004. High-Order Methods for Incompressible Fluid Flow. Cambridge Monographs on Applied and Computational Mathematics. Cambridge University Press.

Ekman, V. W., 1905. On the influence of the Earth's rotation on ocean currents. Ark. Mat. Astron. Fys. 2, 1–53.

Fischer, P. F., 1997. An overlapping Schwarz method for spectral element solution of the incompressible Navier–Stokes equations. Journal of Computational Physics 133 (1), 84–101.

Gray, D. D., Giorgini, A., 1976. The validity of the Boussinesq approximation for liquids and gases. International Journal of Heat and Mass Transfer 19 (5), 545–551.

Grossmann, S., Lohse, D., 2000. Scaling in thermal convection: a unifying theory. Journal of Fluid Mechanics 407, 27–56.

Hartmann, D. L., Moy, L. A., Fu, Q., 2001. Tropical convection and the energy balance at the top of the atmosphere. Journal of Climate 14 (24), 4495–4511.

Hébert, F., Hufschmid, R., Scheel, J., Ahlers, G., Apr 2010. Onset of Rayleigh-Bénard convection in cylindrical containers. Phys. Rev. E 81, 046318.

Horn, S., Shishkina, O., 2014. Rotating non–Oberbeck–Boussinesq Rayleigh–Bénard convection in water. Physics of Fluids (1994-present) 26 (5).

Julien, K., Legg, S., McWilliams, J., Werne, J., 1996a. Hard turbulence in rotating Rayleigh-Bénard convection. Physical Review E 53 (6), R5557.

Julien, K., Legg, S., McWilliams, J., Werne, J., 1996b. Rapidly rotating turbulent Rayleigh-Bénard convection. Journal of Fluid Mechanics 322, 243–273.

Karniadakis, G. E., Israeli, M., Orszag, S. A., 1991. High-order splitting methods for the incompressible Navier–Stokes equations. Journal of Computational Physics 97 (2), 414–443.

Kerr, R. M., 1996. Rayleigh number scaling in numerical convection. Journal of Fluid Mechanics 310, 139–179.

King, E. M., Aurnou, J. M., 2012. Thermal evidence for Taylor columns in turbulent rotating Rayleigh-Bénard convection. Physical Review E 85 (1), 016313.

King, E. M., Soderlund, K. M., Christensen, U. R., Wicht, J., Aurnou, J. M., 2010. Convective heat transfer in planetary dynamo models. Geochemistry, Geophysics, Geosystems 11 (6).

Kundu, P., Cohen, I., 2010. Fluid Mechanics. Elsevier Science.

Kunnen, R. P., Stevens, R. J., Overkamp, J., Sun, C., van Heijst, G. F., Clercx, H. J., 2011. The role of stewartson and ekman layers in turbulent rotating rayleigh–bénard convection. Journal of fluid mechanics 688, 422–442.

Kunnen, R. P. J., Clercx, H. J. H., Geurts, B. J., Nov 2006. Heat flux intensification by vortical flow localization in rotating convection. Phys. Rev. E 74, 056306.

Kunnen, R. P. J., Clercx, H. J. H., Geurts, B. J., 2008. Breakdown of large-scale circulation in turbulent rotating convection. EPL (Europhysics Letters) 84 (2), 24001.

Kunnen, R. P. J., Geurts, B. J., Clercx, H. J. H., 1 2010. Experimental and numerical investigation of turbulent convection in a rotating cylinder. Journal of Fluid Mechanics 642, 445–476.

Landau, L. D., Lifshitz, E. M., 1987. Fluid Mechanics, 2nd Edition. Vol. 6 of Course of Theoretical Physics. Pergamon Press.

Liu, Y., Ecke, R. E., 1997. Heat transport scaling in turbulent Rayleigh-Bénard convection: effects of rotation and Prandtl number. Physical review letters 79 (12), 2257.

Liu, Y., Ecke, R. E., 2009. Heat transport measurements in turbulent rotating Rayleigh-Bénard convection. Physical Review E 80 (3), 036314.

Malm, J., Schlatter, P., Fischer, P. F., Henningson, D. S., 2013. Stabilization of the spectral element method in convection dominated flows by recovery of skew-symmetry. Journal of Scientific Computing 57 (2), 254–277.

Miesch, M. S., 2005. Large-scale dynamics of the convection zone and tachocline. Living Reviews in Solar Physics 2 (1), 1–139.

Niemela, J., Babuin, S., Sreenivasan, K., 2010. Turbulent rotating convection at high Rayleigh and Taylor numbers. Journal of Fluid Mechanics 649, 509–522.

Oberbeck, A., 1879. Ueber die Wärmeleitung der Flüssigkeiten bei Berücksichtigung der Strömungen infolge von Temperaturdifferenzen. Annalen der Physik 243 (6), 271–292.

Rønquist, E. M., 1996. Convection treatment using spectral elements of different order. International Journal for Numerical Methods in Fluids 22 (4), 241–264.

Rossby, H. T., 1969. A study of Bénard convection with and without rotation. Journal of Fluid Mechanics 36, 309–335.

Shraiman, B. I., Siggia, E. D., 1990. Heat transport in high-Rayleigh-number convection. Physical Review A 42 (6), 3650.

Stevens, R. J., Zhong, J.-Q., Clercx, H. J., Ahlers, G., Lohse, D., 2009. Transitions between turbulent states in rotating Rayleigh-Bénard convection. Physical review letters 103 (2), 024503.

Stevens, R. J. A. M., van der Poel, E. P., Grossmann, S., Lohse, D., 9 2013. The unifying theory of scaling in thermal convection: the updated prefactors. Journal of Fluid Mechanics 730, 295–308.

Verzicco, R., Camussi, R., 2003. Numerical experiments on

strongly turbulent thermal convection in a slender cylindrical cell. Journal of Fluid Mechanics 477, 19–49.

Verzicco, R., Orlandi, P., 1996. A finite-difference scheme for three-dimensional incompressible flows in cylindrical coordinates. Journal of Computational Physics 123 (2), 402–414.

Weiss, S., Ahlers, G., 2011. Heat transport by turbulent rotating Rayleigh–Bénard convection and its dependence on the aspect ratio. Journal of Fluid Mechanics 684, 407–426.

Zhong, J.-Q., Stevens, R. J. A. M., Clercx, H. J. H., Verzicco, R., Lohse, D., Ahlers, G., Jan 2009. Prandtl-, Rayleigh-, and Rossby-number dependence of heat transport in turbulent rotating Rayleigh-Bénard convection. Phys. Rev. Lett. 102, 044502.